

Electroweak penguin decays at LHCb

T. Blake on behalf of the LHCb collaboration
CERN, Switzerland

Promising ways to search for New Physics effects in radiative penguin decays are in the angular analysis of $B_d \rightarrow K^{*0}\mu^+\mu^-$, in the measurement of direct CP violation in $B_d \rightarrow K^{*0}\gamma$ and a time dependent analysis of $B_s \rightarrow \phi\gamma$. All of these studies are being pursued at LHCb. First results will be shown from the 2010 and early 2011 data, with particular emphasis on $B_d \rightarrow K^{*0}\mu^+\mu^-$.

1. Introduction

The decay processes $b \rightarrow s\ell^+\ell^-$ and $b \rightarrow s\gamma$ are flavour changing neutral currents that are forbidden at tree level in the Standard Model (SM). These processes can proceed via higher order electroweak Z^0/γ penguin or box diagrams. In extensions to the SM, new virtual particles can enter in competing (loop order) diagrams, leading, in the absence of a dominant SM tree process, to comparably large deviations from SM predictions. These deviations may be: in enhancements (or suppression) of branching fractions; in angular distributions (e.g. $B_d \rightarrow K^{*0}\mu^+\mu^-$); CP or Isospin asymmetries. Rare decay processes provide a complementary approach to direct searches at the general purpose detectors and can provide sensitivity to new particles with masses of up-to $\mathcal{O}(10 - 100 \text{ TeV})$.

The angular analysis of $B_d \rightarrow K^{*0}\mu^+\mu^-$, based on 309 pb^{-1} of integrated luminosity collected by the LHCb experiment in 2011, is described in Sec. 2. More details on the angular analysis of $B_d \rightarrow K^{*0}\mu^+\mu^-$ with this data set can be found in Ref. [1]. Initial studies of $B_d \rightarrow K^{*0}\gamma$ and $B_s \rightarrow \phi\gamma$ based on 88 pb^{-1} of integrated collected in 2010 and 2011 are described in Sec. 3. The search for the rare decay $B_s \rightarrow \mu^+\mu^-$ is described in detail elsewhere in these proceedings [2].

1.1. The LHCb detector

The LHCb detector is a single-arm spectrometer designed to study b -hadron decays with an acceptance for charged tracks with pseudorapidity, η , of $2 < \eta < 5$. Primary proton-proton vertices (PVs), and secondary B -vertices are identified in a silicon strip vertex detector (the VELO) that approaches within 8 mm of the LHC beam. Tracks from charged particles are reconstructed in the vertex detector and a set of tracking stations and their curvature in the dipole magnet allows momenta to be determined with a precision of $\delta p/p = 0.35\text{--}0.5\%$. Two Ring Imaging Cherenkov (RICH) detectors allow for charged hadrons to be separated over a momentum range $2 \text{ GeV}/c < p < 100 \text{ GeV}/c$. Muons with momentum above $3 \text{ GeV}/c$ are identified on the basis of the number of hits left in detectors interleaved with an iron muon filter. Further details on the LHCb detector can be found in Ref. [3]. Key for the rare electroweak penguin processes are the excellent momentum and mass resolution provided by the long lever arm for tracking, the primary-secondary vertex separation provided by the VELO and the ability to reject a range of exclusive backgrounds provided by LHCb's RICH detectors.

1.2. LHCb data taking performance in 2011

In the first three months of data taking in 2011, LHCb accumulated $\sim 300 \text{ pb}^{-1}$ of integrated luminosity at $\sqrt{s} = 7 \text{ TeV}$. This luminosity was delivered by the LHC at instantaneous luminosities of $3 \times 10^{32} \text{ cm}^{-2}\text{s}^{-1}$, 50% above the original design luminosity of LHCb. At this instantaneous luminosity, it is expected that LHCb will collect $\mathcal{O}(1 \text{ fb}^{-1})$ of integrated luminosity in 2011.

2. The decay $B_d \rightarrow K^{*0} \mu^+ \mu^-$

The decay $B_d \rightarrow K^{*0} \mu^+ \mu^-$ is an example of a $b \rightarrow s \ell^+ \ell^-$ process that can be a highly sensitive probe of new right-handed currents and large contributions from new scalar or pseudo-scalar couplings. In many models these new virtual particles give rise to modifications in the distribution of the daughters of the B_d that can be probed through an angular analysis. To achieve ultimate sensitivity, the long term goal of LHC**b** is to perform a full angular analysis of the decay [4]. However, with more modest data sets, the focus is instead on observables that are theoretically clean and can be extracted from simple counting experiments or from simple fits to angular distributions. One such observable, that is widely discussed in the literature, is the forward-backward asymmetry of the muon system (A_{FB}). A_{FB} varies with the invariant mass-squared of the dimuon pair (q^2) and in the SM changes sign at a well defined point, where the leading hadronic uncertainties cancel. In many NP models the shape of A_{FB} as a function of q^2 can be dramatically altered. The variation of $A_{FB}(q^2)$ in the SM and several NP models in the low- q^2 region, from Ref. [5], are shown in Fig. 1

Recent measurements from BABAR [6], Belle [7] and CDF [8] have generated excitement as they appear to favour a forward-backward asymmetry with the opposite sign to the SM prediction at low- q^2 and no zero-crossing point.

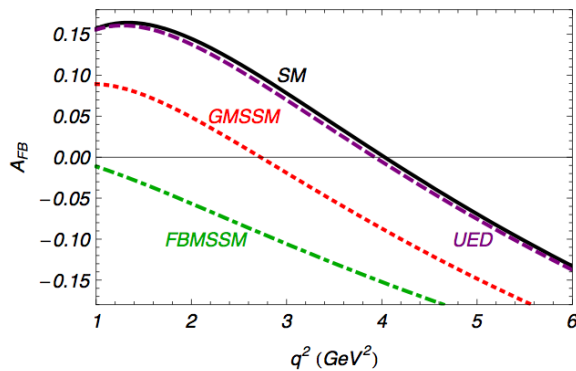


Figure 1: The forward backward asymmetry of muons in $B_d \rightarrow K^{*0} \mu^+ \mu^-$ as a function of $q^2 = m_{\mu^+ \mu^-}^2$ predicted in the SM (solid-black line) and a variety of NP models. The SM prediction and the NP models are described in detail in Ref. [5].

In 309 pb^{-1} LHC**b** observes 302 ± 20 candidates in a $\pm 50 \text{ MeV}/c^2$ $K^\pm \pi^\mp \mu^+ \mu^-$ mass window. Candidates were triggered by: a single high- p_T muon in LHC**b**'s Level0 hardware trigger [9]; a single high impact parameter and high- p_T daughter [10] in the first stage of a two stage software trigger and ‘topologically’ by partially reconstructing the B_d decay in the second stage of the software trigger [11].

Offline, candidates are first selected by applying a loose pre-selection based on the B_d lifetime, daughter impact parameters and a requirement that the B_d points back to one of the primary vertices in the event. A multivariate selected based on a Boosted Decision Tree (BDT) was then used to further reduce combinatorial background. The BDT combined information on the B_d kinematics, B_d vertex quality, and the kaon, pion and muon impact parameter and particle identification. The BDT allowed a signal-to-background ratio of three-to-one to be achieved across the $\pm 50 \text{ MeV}/c^2$ signal mass window. The multivariate selection was trained using $B_d \rightarrow K^{*0} J/\psi$ candidates and background from the upper mass sideband of a 36 pb^{-1} data set collected in 2010. These events are not used in the subsequent analysis. Care has also been taken to avoid further biasing the angular distribution in the offline selection.

Specific exclusive backgrounds from, e.g, $B_d \rightarrow J/\psi (\rightarrow \mu^+ \mu^- \{ \pi^- \}) K^{*0} (\rightarrow K^+ \pi^- \{ \mu^- \})$ where the pion from the K^{*0} is misidentified as a muon and a muon from the J/ψ as the pion, are removed by exchanging the mass assignments of the daughters and cutting on the the resulting B_d mass in combination with cuts on the daughter particle identification. These selection criteria are almost 100% efficient on genuine $B_d \rightarrow K^{*0} \mu^+ \mu^-$ candidates and reduce this type of background to a negligible level. In particular the exclusive background from

$B_d \rightarrow K^{*0} \mu^+ \mu^-$ where the K^{*0} is misidentified as a \bar{K}^{*0} is reduced to 1% of the level of the signal, diluting the measured A_{FB} by 2%. This dilution is accounted for in the results presented below. The regions around the J/ψ and $\psi(2S)$ are also removed as they are dominated by different physics from $c\bar{c}$ loops (see Fig. 2).

The forward backward-asymmetry (A_{FB}) of the muon system is extracted from the angular distribution of the μ^+ (μ^-) helicity angle w.r.t. the dimuon flight direction in the rest-frame of the B_d (\bar{B}_d). The probability density distribution for the cosine of this angle, $\cos \theta_\ell$ is given by:

$$\frac{1}{\Gamma} \frac{d^2\Gamma}{d \cos \theta_\ell dq^2} = \frac{3}{4} F_L (1 - \cos^2 \theta_\ell) + \frac{3}{8} (1 - F_L) (1 + \cos^2 \theta_\ell) + A_{FB} \cos \theta_\ell \quad (1)$$

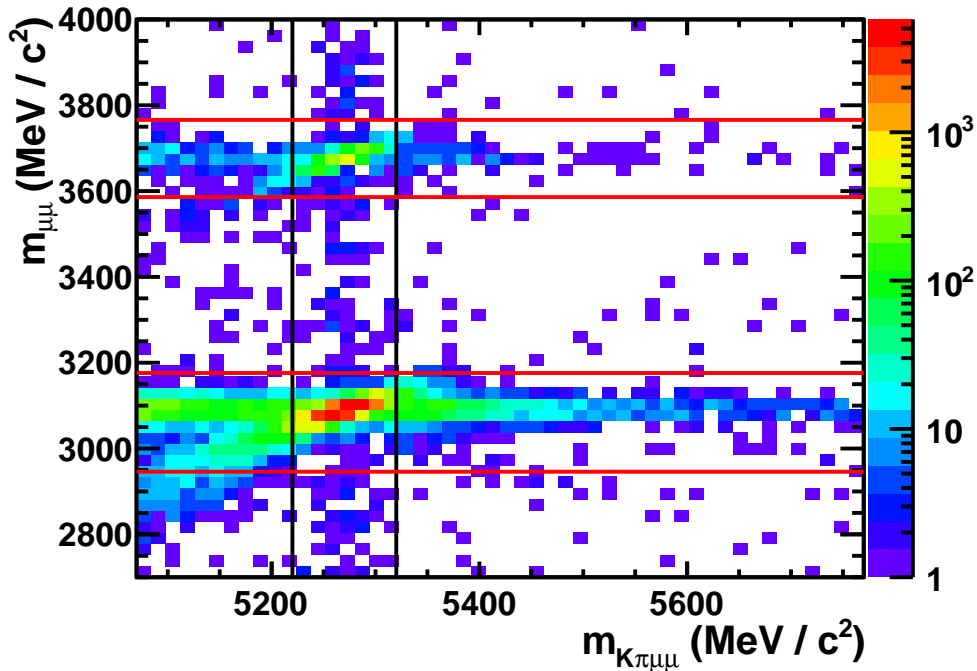


Figure 2: Scatter plot highlighting the correlation between $m_{\mu^+\mu^-}$ and $m_{K\pi\mu\mu}$ for candidates used in the analysis. The vertical band illustrates the $\pm 50 \text{ MeV}/c^2$ signal mass window used in the analysis. The horizontal bands illustrate the J/ψ and $\psi(2S)$ regions that are treated separately in the analysis. A clear $B_d \rightarrow K^{*0} \mu^+ \mu^-$ signal is visible across $m_{\mu^+\mu^-}$, centered on the B_d mass.

which also depends on F_L , the fraction of longitudinal polarisation of the K^{*0} . F_L is constrained by simultaneously fitting the helicity angle of the kaon (θ_K). The probability density function for $\cos \theta_K$ only depends on F_L and is given by:

$$\frac{1}{\Gamma} \frac{d^2\Gamma}{d \cos \theta_K dq^2} = \frac{3}{2} F_L \cos^2 \theta_K + \frac{3}{4} (1 - F_L) (1 - \cos^2 \theta_K) \quad (2)$$

The analysis is performed in six- q^2 bins, chosen for consistency to be the same binning scheme used by previous experiments. A significant $B_d \rightarrow K^{*0} \mu^+ \mu^-$ signal is visible in each of the six bins with an excellent signal-to-background ratio even in the lowest q^2 bin (see Fig. 3).

Unfortunately the extraction of A_{FB} is complicated by a correlation between A_{FB} and F_L that prevents the A_{FB} from being large if F_L is also large. The allowed region of phase space, where Eq. 1 remains positive and well defined, corresponds to $|A_{FB}| \leq \frac{3}{4}(1 - F_L)$. To account for the ‘physical’ region a profile likelihood scan is made over the plane, with a flat prior that the maximum likelihood must lie in the physical region. The statistical uncertainty on the central value of A_{FB} and F_L is calculated by integrating the likelihood to yield an (asymmetric) 68% confidence limit on A_{FB} and F_L .

The fit results for A_{FB} and F_L in six q^2 bins are shown in Fig. 4 along with the differential branching fraction of $B_d \rightarrow K^{*0} \mu^+ \mu^-$ as a function of q^2 . The differential branching fraction is extracted from fits to the $K^\pm \pi^\mp \mu^+ \mu^-$ mass distribution in the q^2 bins and normalised with respect to the branching fraction of $B_d \rightarrow J/\psi K^{*0}$.

The systematic uncertainties on A_{FB} , F_L and the differential branching fraction are typically 30% of the statistical uncertainty. Across q^2 a dominant contribution to the systematic uncertainty comes from the understanding of data-derived corrections to the detector performance, which is expected to improve with increased statistics. The choice of the background angular and mass model in the fit for A_{FB} and F_L lead to a systematic uncertainty at the level of 10-20% of the statistical uncertainty. This model dependence will also improve with an enlarged data set.

The observed forward-backward asymmetry, longitudinal K^{*0} polarisation and differential branching fraction are consistent with a SM interpretation. In particular the observed forward-backward asymmetry shows evidence for a zero-crossing point which could be measured with a larger data set.

3. Radiative decays in LHCb

The long term goal of the LHCb radiative decay program is a measurement of the right-handed component of the photon polarization, probed using a time dependent analysis of $B_s \rightarrow \phi \gamma$ decays [13]. In the shorter term, a

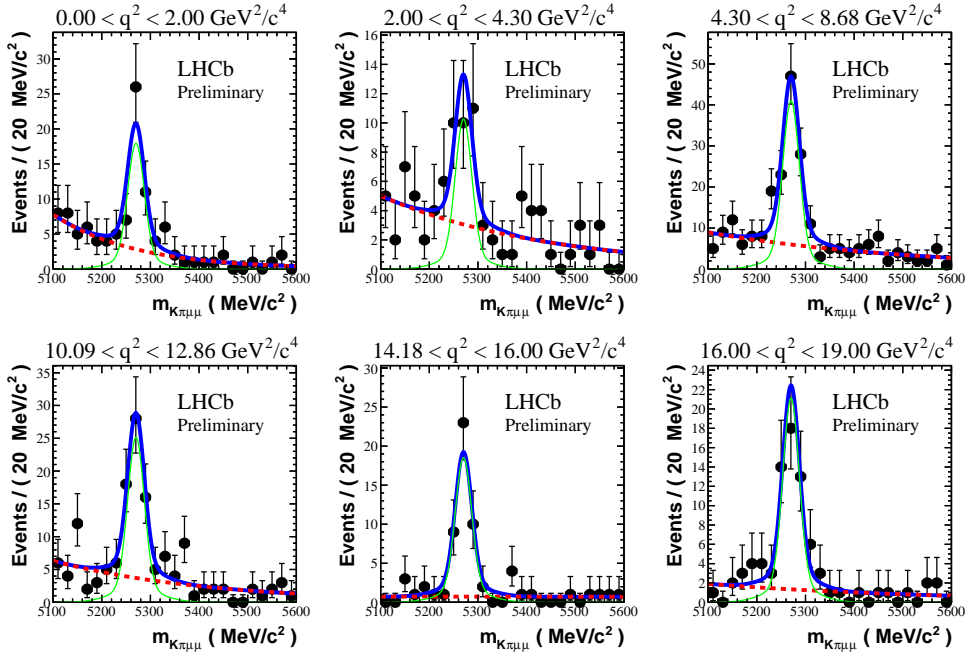


Figure 3: The $K^\pm \pi^\mp \mu \mu$ mass distribution of $B_d \rightarrow K^{*0} \mu^+ \mu^-$ candidates in six q^2 bins. The solid line shows a fit to this distribution with a double-Gaussian signal component (thin-green line) and Exponential background component (dashed-red line).

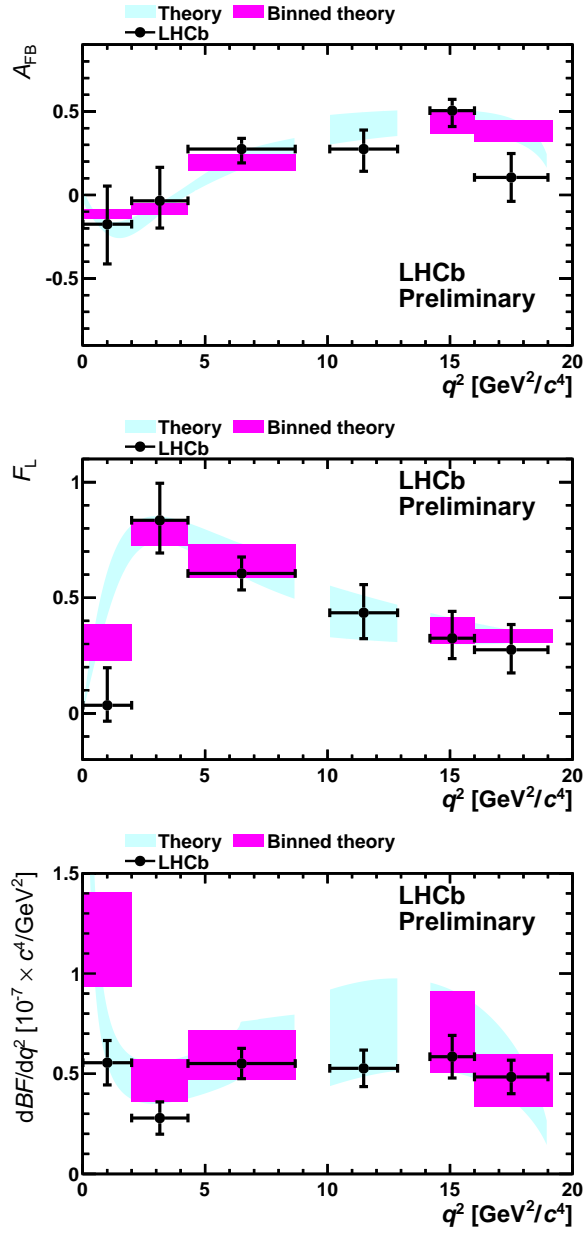


Figure 4: A_{FB} , F_L and the differential branching fraction of $B_d \rightarrow K^{*0} \mu^+ \mu^-$ candidates as a function of q^2 in the six q^2 bins. The theory predictions are described in Ref. [12]

large $B_d \rightarrow K^{*0} \gamma$ yield will enable LHCb to make a world leading measurement of the $\mathcal{A}_{CP}(B_d \rightarrow K^{*0} \gamma)$. The most precise single measurement of $\mathcal{A}_{CP}(B_d \rightarrow K^{*0} \gamma)$ comes from the BABAR experiment, based on 2400 B_d candidates [14]. A large $B_s \rightarrow \phi \gamma$ could allow an improved measurement of the $B_s \rightarrow \phi \gamma$ branching fraction.

In 88 pb^{-1} collected by LHCb in 2010 and 2011, LHCb observes 485 ± 43 $B_d \rightarrow K^{*0} \gamma$ candidates and 60 ± 12 $B_s \rightarrow \phi \gamma$ candidates. The $B_s \rightarrow \phi \gamma$ yield is the largest yield of B_s radiative decays at a single experiment. The $K^\pm K^\mp \gamma$ and $K^\pm \pi^\mp \gamma$ mass distributions of these candidates is shown in Fig. 5. The reconstructed $K^\pm K^\mp \gamma$ and $K^\pm \pi^\mp \gamma$ signal mass resolution is $\sim 125 \text{ MeV}/c^2$. This is larger than the Monte Carlo prediction of $100 \text{ MeV}/c^2$,

but will improve with ongoing (time-dependent) Calorimeter calibration.

$B_d \rightarrow K^{*0}\gamma$ and $B_s \rightarrow \phi\gamma$ candidates are triggered in LHCb's Level-0 hardware trigger on the high- E_T photon or by the kaon or pion from the ϕ or K^{*0} [9]. In the first stage of the software trigger the events are triggered by a high- p_T and high-IP track (from the ϕ or K^{*0}) or by a softer track and a high- E_T photon. In the second stage of the software trigger a full exclusive reconstruction of the B is performed which mirrors the offline selection.

The offline selection is similar to the pre-selection of $B_d \rightarrow K^{*0}\mu^+\mu^-$ described above in that the tracks from the K^{*0} and ϕ are required to have significant impact parameter and the B is required to point back to the PV. Additional requirements are then made of the γ p_T ($p_T > 2.6$ GeV/ c) and on the B p_T ($p_T > 3$ GeV/ c) and isolation to improve the purity of the signal.

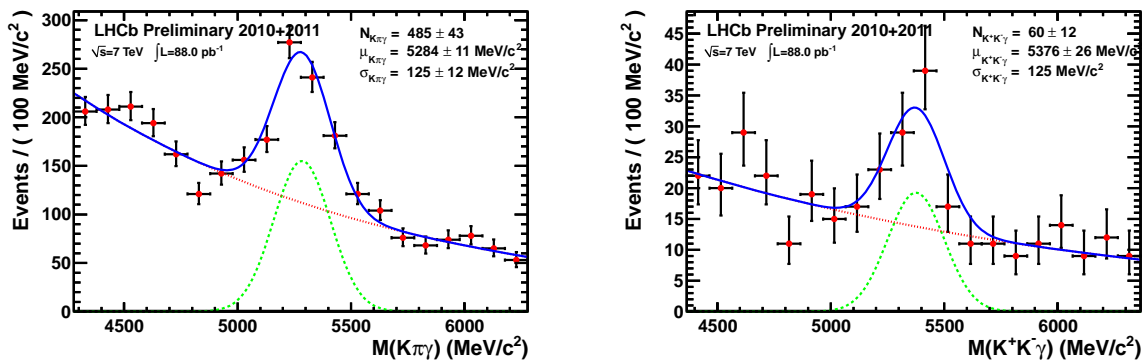


Figure 5: Reconstructed $K^\pm\pi^\mp\gamma$ (top) and $K^\pm K^\mp\gamma$ mass distributions in 88 pb^{-1} of integrated luminosity. The solid line is a fit to the data with a Gaussian signal distribution (green-dotted line) and exponential background distribution (red-thin line)

Extrapolating to a 1 fb^{-1} data set, LHCb expects to collect a data sample of $\mathcal{O}(5000)$ $B_d \rightarrow K^{*0}\gamma$ candidates and $\mathcal{O}(700)$ $B_s \rightarrow \phi\gamma$ candidates, which would also represent the largest sample of radiative B_d decays at a single experiment.

4. Summary

In 2011 the performance of the LHC and LHCb has been excellent delivering 300 pb^{-1} of integrated luminosity in the first three months of data taking. This data sample has enabled LHCb to make the world's most precise measurement of the $A_{FB}(q^2)$ in $B_d \rightarrow K^{*0}\mu^+\mu^-$, which shows a striking agreement with the SM prediction. By the end of 2011, it is expected that LHCb will have recorded 1 fb^{-1} of integrated luminosity providing

the worlds largest samples of reconstructed $B_d \rightarrow K^{*0}\gamma$ and $B_s \rightarrow \phi\gamma$ decays. This expanded data set will also enable LHC**b** to make a first measurement of the forward-backward asymmetry zero-crossing point and transverse asymmetries [4] in $B_d \rightarrow K^{*0}\mu^+\mu^-$ and to pursue a wide range of other rare decay measurements.

Acknowledgments

We express our gratitude to our colleagues in the CERN accelerator departments for the excellent performance of the LHC. We thank the technical and administrative staff at CERN and at the LHC**b** institutes, and acknowledge support from the National Agencies: CAPES, CNPq, FAPERJ and FINEP (Brazil); CERN; NSFC (China); CNRS/IN2P3 (France); BMBF, DFG, HGF and MPG (Germany); SFI (Ireland); INFN (Italy); FOM and NWO (Netherlands); SCSR (Poland); ANCS (Romania); MinES of Russia and Rosatom (Russia); MICINN, XUNGA and GENCAT (Spain); SNSF and SER (Switzerland); NAS Ukraine (Ukraine); STFC (United Kingdom); NSF (USA). We also acknowledge the support received from the ERC under FP7 and the Région Auvergne.

References

- 1 The LHC**b** collaboration, CERN-LHC**b**-CONF-2011-038 (2011).
- 2 M-O. Bettler, these proceedings.
- 3 A. A. Alves Jr. *et al.*, JINST **3** S08005 (2008).
- 4 U. Egede *et al.*, JHEP 1010:056 (2010).
- 5 W. Altmannshofer *et al.*, JHEP 0901:019 (2009).
- 6 B. Aubert *et al.*, Phys. Rev. D. **79** (2009).
- 7 J.-T. Wei *et al.*, Phys. Rev. Lett. **103** (2009).
- 8 T. Aaltonen *et al.*, Phys. Rev. Lett. **106** (2011).
- 9 The LHC**b** collaboration, CERN-LHCC-2003-031(2003).
- 10 V. V. Gligorov *et al.*, CERN-LHC**b**-PUB-2011-003 (2011).
- 11 M. Williams *et al.*, CERN-LHC**b**-PUB-2011-002 (2011).
- 12 C. Bobeth *et al.*, arXiv:1105.0376 (2011). U. Egede *et al.*, JHEP 0811:032 (2008).
- 13 R. Zwicky *et al.*, Phys. Lett. B. **664** (2008).
- 14 B. Aubert *et al.*, Phys. Rev. D. **103** (2009).